

Short communication

Role of ceria in the improvement of SO₂ resistance of La_xCe_{1-x}FeO₃ catalysts for catalytic reduction of NO with CO



Yihong Qin, Ligu Sun*, Danglong Zhang, Lei Huang

School of Metallurgy and Environment, Central South University, Changsha, Hunan, PR China

ARTICLE INFO

Article history:

Received 28 December 2015

Received in revised form 7 March 2016

Accepted 8 March 2016

Available online 10 March 2016

Keywords:

Perovskite

LaFeO₃ catalyst

Ce

SO₂ resistance

Selective catalytic reduction

ABSTRACT

Perovskite-type catalysts with LaFeO₃ and substituted La_xCe_{1-x}FeO₃ compositions were prepared by sol-gel method. These catalysts were characterized by X-ray diffraction (XRD), X-ray photoelectron spectroscopy (XPS), CO temperature-programmed reduction (CO-TPR), and SO₂ temperature-programmed desorption (SO₂-TPD). Catalytic reaction for NO reduction with CO in the presence of SO₂ has been investigated in this study. LaFeO₃ exhibited an excellent catalytic activity without SO₂, but decreased sharply when SO₂ gas was added to the CO + NO reaction system. In order to inhibit the effect of SO₂, substitution of Ce in the structure of LaFeO₃ perovskite has been investigated. It was found that La_{0.6}Ce_{0.4}FeO₃ showed the maximum SO₂ resistance among a series of La_xCe_{1-x}FeO₃ composite oxides.

© 2016 Elsevier B.V. All rights reserved.

1. Introduction

Emissions of nitrogen oxides (NO and NO₂) in urban area have resulted in severe environmental conditions such as acid rain and fog and haze worldwide [1]. Reduction of nitrogen oxide to nitrogen is the most promising process to control NO_x emissions. Selective catalytic reduction of NO by NH₃ (NH₃-SCR) has been proved an effective method for the removal of NO at low temperatures [2]. However, NH₃ is very sensitive to the reaction temperature and atmosphere; furthermore, it is expensive and inconvenient for industrial application. Catalytic reduction of NO by CO is a key chemical process, because it eliminates both NO and CO emissions. Because it uses CO as reductant, one of the usual components of exhaust gases, this process is not affected by the possible slipping of NH₃ [3].

The highly increasing demand for NO reduction, which is one of the most important tasks for the control of air pollution, has led to the development of new catalysts. Noble metals (e.g., Pt and Pd) and their oxides were previously investigated as catalyst for the reduction of NO [4–5]. However, these catalysts usually tend to collapse the structure of the reactants at high temperatures or easily agglomerated during the reaction. Perovskite-type mixed oxides of the general-type ABO₃ have been widely studied for their unique physical and chemical properties. In this particular structure, A is the larger cation with 12-fold coordination and B is the smaller cation with six fold coordination [6]. Compared with noble metals,

perovskite-type oxides can select low-cost elements to replace the sites of A or B, and be stable even above 1000 °C. Redox properties of these oxides could be modified by the substitution of A- or B-site cation, without destroying the matrix perovskite structure, and oxygen vacancy will be created to meet the chemical charge valence of the perovskite structure [7]. This vacancy could significantly enhance the redox properties of the catalyst. Thus, it is evident that perovskite-type oxides could be a potential catalyst for NO reduction.

A substantial amount of SO₂ gases exists in most industrial exhaust gases, because of the presence of sulfur in fossil fuel. The negative effect of SO₂ restricts the practical application of NO reduction. SO₂ could form sulfide and sulfate species on the catalyst surface, which is harmful to the catalytic reaction [8–9]. Therefore, it is necessary to improve SO₂ resistance of the catalysts. Ceria has two different valences Ce³⁺ and Ce⁴⁺, and is thus capable of storing and releasing oxygen via redox shift under oxidizing or reducing conditions [10–11]. Considering its particular redox property, A-site substitution with Ce in ABO₃ perovskite structure could be a potential way to enhance SO₂ resistance of ABO₃ perovskite catalyst.

In this study, LaFeO₃ and a series of La_xCe_{1-x}FeO₃ perovskite-type oxide catalysts were prepared by citric acid sol-gel method. All these samples were characterized by X-ray diffraction (XRD), Brunauer-Emmett-Teller (BET) method, X-ray photoelectron spectroscopy (XPS), SO₂ temperature-programmed desorption (SO₂-TPD) and CO temperature-programmed reduction (CO-TPR) to illustrate the influence of Ce substitution on SO₂ resistance, and explain the role played by Ce in La_xCe_{1-x}FeO₃ perovskite-type catalyst.

* Corresponding author.

E-mail address: sunliguo411@gmail.com (L. Sun).

2. Experimental

2.1. Catalyst preparation

LaFeO₃ samples were prepared by a citric acid sol–gel method. Equal amounts of lanthanum nitrate and ferric nitrate were dissolved in deionized water and mixed together, and then 120% (molar ratio) of citric was added into the solution and stirred for 30 min. The solution was evaporated at 80 °C until it became viscous. The obtained sample was dehydrated at 120 °C for 12 h, and then calcined in airflow at 750 °C for 4 h. La_xCe_{1-x}FeO₃ samples were synthesized by the same way. The proportions of lanthanum nitrate and ceria nitrate varied according to the value of x in each La_xCe_{1-x}FeO₃ sample. This process is similar to the LaFeO₃ synthesis process, except the addition of ceria nitrate in the first step.

2.2. Characterization

XRD patterns were acquired using a Rigaku-TTRIII diffract meter operating at 40 kV and 40 mA with nickel-filtered Cu K_α radiation ($\lambda = 1.5418 \text{ \AA}$) in the range of $10^\circ \leq \theta \leq 80^\circ$, at a step size of 0.02°.

BET surface area was determined by N₂ at 77 K using a Micrometrics ASAP-2020 analyzer. Before each adsorption measurement, approximately 0.1 g of the catalyst sample was degassed in a N₂/He mixture at 300 °C for 4 h.

The CO-TPR was measured using 1% CO/Ar and 0.1 g of catalyst at a total flow rate of 100 ml/min. Before TPR measurements, the catalyst was pretreated in a flow of O₂ at 500 °C for 30 min, followed by cooling to room temperature. The catalyst was placed in a quartz tube surrounded by a tube furnace, and the temperature was increased to 1000 °C at a rate of 10 °C/min. The outlet gas was monitored by Autochem2920 (Micrometrics).

SO₂-TPD was performed with 0.5 g of the catalyst sample at a total flow rate of 100 ml/min. Before TPD measurements, the catalysts were pretreated in a flow of O₂ at 500 °C for 30 min and then cooled to room temperature. The samples were then treated with 1% SO₂/Ar for 1 h. The SO₂ was purged with Ar for 1 h before starting the TPD experiments. During the TPD experiments, the temperature was increased to 1000 °C at a rate of 10 °C/min, the SO₂ outlet gas was monitored by a thermal conductivity (TC) detector.

XPS experiments were performed on a PHI-5300 ESCA system with Al K radiation under ultrahigh vacuum (UHV, 1.33×10^{-8} Pa). Before the measurement, the sample was outgassed at room temperature in a UHV chamber ($<5 \times 10^{-7}$ Pa). All peaks were calibrated by the carbon deposit C 1s binding energy (BE) at 284.8 eV. The atomic ratios were calculated by using the atomic sensitivity factors provided by the manufacturer.

2.3. Activity test

Catalytic reaction was carried out in a quartz tube (d = 6 mm; l = 60 mm), and the catalyst samples (500 mg) were placed in the middle of the tube. The simulated flue gas was a mixture of NO (400 ppm), CO (500 ppm), SO₂ (100 ppm when needed), O₂ (3%), and water (3 vol.%) with balance N₂, while gas hourly space velocity (GHSV) = 24,000 h⁻¹. Then the quartz tube was heated to increase the temperature from 100 to 500 °C. The outlet gases NO and NO₂ were analyzed by MRU VarioPlus, and N₂O was measured by Nicolet 380. The NO conversions and N₂ selectivity of the catalyst were calculated by the following equations:

$$\text{NO conversion (\%)} = \frac{\text{NO in} - \text{NO out} - \text{NO}_2 \text{ out} - \text{N}_2\text{O out}}{\text{NO in}} \times 100\% \quad (1)$$

$$\text{N}_2 \text{ selectivity (\%)} = \frac{\text{NO in} - \text{NO out} - \text{NO}_2 \text{ out} - \text{N}_2\text{O out}}{\text{NO in} - \text{NO out}} \times 100\% \quad (2)$$

3. Results and discussion

3.1. Catalytic activity results

Fig. 1 shows the NO conversion rate of the La_xCe_{1-x}FeO₃ samples with different amounts of Ce substitution. Fig. 1a and c shows the results of NO conversion and N₂ selectivity for NO + CO reaction, respectively, with La_xCe_{1-x}FeO₃ samples and reaction temperature ranging from 100 to 500 °C. Without the addition of SO₂, the LaFeO₃ catalyst exhibited the maximum catalytic performance, the maximum conversion rate of 100% at 500 °C and N₂ selectivity of approximately 80%.

Fig. 1b shows the effect of SO₂ in NO reduction with CO. The long time durable experiment started with CO + NO mixed gases, whose temperature was maintained at 500 °C. After 30 min, a certain amount of SO₂ (100 ppm) was added into the mixed gases system, and the catalytic activity started changing, which is attributed to the influence of SO₂ injection. As mentioned earlier, the LaFeO₃ sample exhibited the maximum NO conversion in the first 30 min; however, after the addition of SO₂, the catalytic performance rapidly declined. After approximately 100 min, catalytic conversion rate of the LaFeO₃ sample decreased to approximately 40–50%. When a certain amount of Ce was introduced into the LaFeO₃ perovskite structure, the SO₂ resistance of the catalysts obviously improved. In particular, the La_{0.6}Ce_{0.4}FeO₃ sample maintained a conversion rate of 80% during the latter 270 min after addition of SO₂ gas into the CO + NO reaction system. However, too much Ce decreases the catalytic ability of La_xCe_{1-x}FeO₃ catalysts, and the conversion rate curve indicates that La_{0.2}Ce_{0.8}FeO₃ and pure CeO₂ samples exhibited poor performance for NO reduction.

Fig. 1d illustrates the NO conversion curves of CO + NO reaction with SO₂, O₂, and H₂O. The catalysts were tested in a mixed gas condition consisting of NO (400 ppm), CO (500 ppm), SO₂ (100 ppm), O₂ (3%), and water (3 vol.%). The catalytic data curves in Fig. 1b and d indicate that SO₂ exhibits poisoning effect on NO reduction. In general, La_{0.6}Ce_{0.4}FeO₃ exhibited both comparatively good catalytic performance for NO reduction and excellent SO₂ resistance to the catalytic reaction.

3.2. Physical properties

Fig. 2 shows the XRD results of LaFeO₃, La_{0.6}Ce_{0.4}FeO₃ and CeO₂ samples. The LaFeO₃ perovskite phase (JCPDS-ICDD, 88-0641) was clearly observed without any segregated phase, with the main peak at 32.3° [12–13]. A single CeO₂ phase (JCPDS-ICDD, 65-5923) was observed at its main peak when diffraction $2\theta = 28.6^\circ$ [14]. For the La_{0.6}Ce_{0.4}FeO₃ sample, the substitution of Ce showed both typical LaFeO₃ perovskite and CeO₂ peaks in its diffraction patterns. Peaks at 28.6° and 32.3° indicated the effect of Ce substitution on the LaFeO₃ perovskite structure.

The BET results are shown in Table 1. Pure LaFeO₃ and CeO₂ have comparatively small surface areas. When Ce was doped in LaFeO₃ perovskite, the surface area and pore volume of La_{0.6}Ce_{0.4}FeO₃ were increased. This increase might be attributed to the substitution of Ce in A-site of LaFeO₃ perovskite [15]. Obviously, a larger surface of the catalyst is beneficial to the absorption and desorption of the reaction gases, which could enhance the catalytic performance to a higher extent.

3.3. CO-TPR

Fig. 3 shows the CO-TPR results of fresh and sulfated samples of LaFeO₃ and La_{0.6}Ce_{0.4}FeO₃. The pure LaFeO₃ sample showed a broad peak at approximately 700 °C, mainly attributed to the reduction of Fe³⁺ [16]. When a certain amount of Ce was introduced into the LaFeO₃ perovskite structure, the consumption of CO slightly increased, and the peak position in temperature did not change. The increase of CO consumption might be attributed to the substitution of Ce.

In order to investigate the effect of SO₂ on the redox property of the catalyst, sulfated samples were also characterized by CO-TPR. For sulfated LaFeO₃ samples, the TPR spectra peak moved forward to

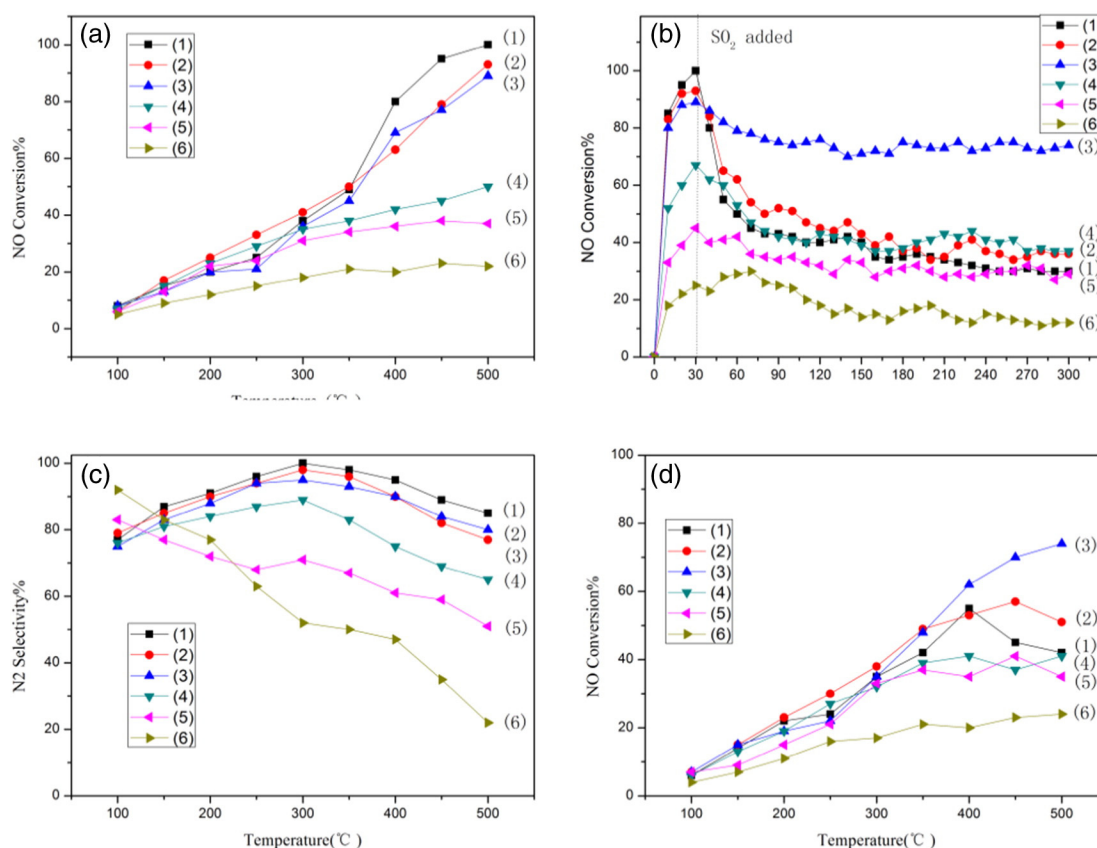


Fig. 1. NO conversion of $\text{La}_x\text{Ce}_{1-x}\text{FeO}_3$ samples in the reaction of catalytic reduction NO with CO. (1) LaFeO_3 , (2) $\text{La}_{0.8}\text{Ce}_{0.2}\text{FeO}_3$, (3) $\text{La}_{0.6}\text{Ce}_{0.4}\text{FeO}_3$, (4) $\text{La}_{0.4}\text{Ce}_{0.6}\text{FeO}_3$, (5) $\text{La}_{0.2}\text{Ce}_{0.8}\text{FeO}_3$, and (6) CeO_2 . (a) NO conversion of $\text{La}_x\text{Ce}_{1-x}\text{FeO}_3$ catalysts in CO + NO reaction from 100 °C to 500 °C. (b) NO conversion of $\text{La}_x\text{Ce}_{1-x}\text{FeO}_3$ catalysts at 500 °C with 100 ppm SO_2 . (c) N_2 selectivity of $\text{La}_x\text{Ce}_{1-x}\text{FeO}_3$ catalysts in CO + NO reaction from 100 °C to 500 °C. (d) NO conversion of $\text{La}_x\text{Ce}_{1-x}\text{FeO}_3$ catalysts in CO + NO reaction with 100 ppm SO_2 , 3% O_2 , 3 vol.% water, from 100 °C to 500 °C.

approximately 600 °C, and the amount of CO consumption sharply decreased, compared with the fresh one. This result indicated that SO_2 could inhibit the redox activity of LaFeO_3 . However, the used $\text{La}_{0.6}\text{Ce}_{0.4}\text{FeO}_3$ sample showed different features in its CO-TPR curve. Compared with the fresh $\text{La}_{0.6}\text{Ce}_{0.4}\text{FeO}_3$ sample, the curve peak of the sulfated sample moved to a lower temperature region, but the amount of CO consumption did not decrease much in the presence of SO_2 . Thus, the results of comparison curve results illustrated an excellent

SO_2 resistance of the $\text{La}_{0.6}\text{Ce}_{0.4}\text{FeO}_3$ sample; its catalytic redox ability was constant when SO_2 gas was added into the selective catalytic reduction system.

3.4. SO_2 -TPD

In order to investigate the effect of SO_2 on the catalyst, the SO_2 -TPD experiments were carried out with the LaFeO_3 and $\text{La}_{0.6}\text{Ce}_{0.4}\text{FeO}_3$ samples. The two desorption curves are shown in Fig. 4. Two obvious peaks were observed for the LaFeO_3 sample. The low-temperature peak at 300–500 °C attributed to the desorption of SO_2 adsorbed in the catalyst surface, and the high-temperature peak between 700 and 900 °C could be attributed to the desorption of SO_2 adsorbed in the subsurface layers or the interior of the catalyst [17–18]. Compared with LaFeO_3 , the $\text{La}_{0.6}\text{Ce}_{0.4}\text{FeO}_3$ sample showed one significant peak at approximately 700 °C, originated from the decomposition of sulfated ceria species $\text{Ce}(\text{SO}_4)_2$, and the amount of SO_2 desorption was relatively less. The TPD spectra of $\text{La}_{0.6}\text{Ce}_{0.4}\text{FeO}_3$ indicated that the addition of ceria to LaFeO_3 perovskite inhibited the reaction with SO_2 , which could prevent the adverse effects of SO_2 to the catalytic redox reaction. This result confirmed the excellent SO_2 resistance of the catalyst.

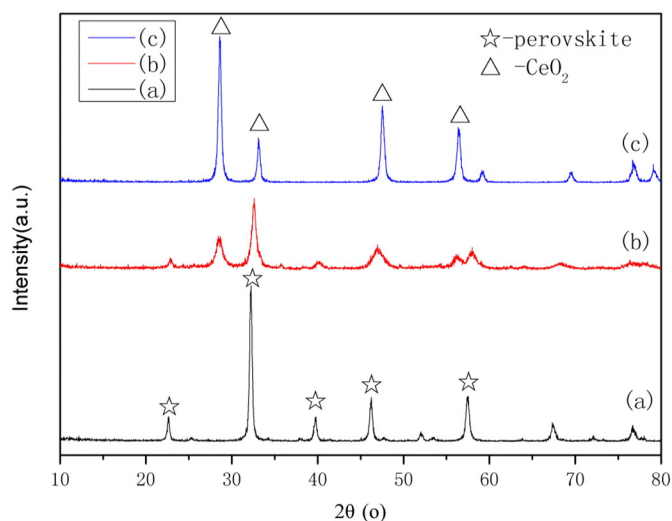


Fig. 2. XRD patterns of (a) LaFeO_3 (b) $\text{La}_{0.6}\text{Ce}_{0.4}\text{FeO}_3$ and (c) CeO_2 samples.

Table 1
Textual properties and crystallite size of different catalyst samples.

Samples	BET surface area (m^2/g)	Pore volume (cm^3/g)	Pore diameter (nm)	Crystallite size (nm)
LaFeO_3	11.3	0.116	1.877	50.4
$\text{La}_{0.6}\text{Ce}_{0.4}\text{FeO}_3$	23.4	0.125	1.732	34.8
CeO_2	6.7	0.168	3.226	12.5

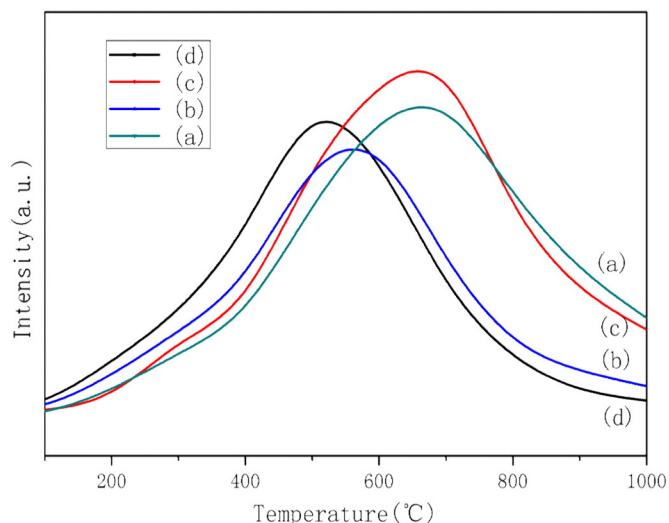


Fig. 3. CO-TPR profiles of (a) LaFeO₃, (b) used LaFeO₃, (c) La_{0.6}Ce_{0.4}FeO₃, (d) used La_{0.6}Ce_{0.4}FeO₃.

3.5. XPS analysis

Ce often appeared as a crucial component for catalysts in selective catalytic reduction, because of its unique redox property. The valence state of the specific element is important to the catalytic reaction. Ce has two different valence states Ce⁴⁺ or Ce³⁺. Therefore, XPS experiments were performed to investigate the surface component and chemical state change of Ce over the La_{0.6}Ce_{0.4}FeO₃ sample. The XPS curves are shown in Fig. 5, and the peaks are fitted by Gaussian–Lorentz curves. The Ce 3d peaks were fitted into sub-bands by searching for the optimum combination of Gaussian bands. The multiple spectra of Ce 3d were decomposed into eight components by the Gaussian–Lorentz fitting procedure. The bands labeled u were due to 3d_{3/2} spin orbit states and those labeled v represented 3d_{5/2} states. The bands labeled as u1 and v1 were attributed to the primary photoemission of Ce³⁺ and the other six bands labeled as u2, v2, u3, v3, u and v were attributed to Ce⁴⁺ [19]. The fitting results revealed that both Ce³⁺ and Ce⁴⁺ exist in the sample. From the peak areas of each state, Ce in the catalyst is mainly in the valence state of +4, and the corresponding results of Ce⁴⁺/Ce³⁺ + Ce⁴⁺ ratio 82.4% were calculated by using the program

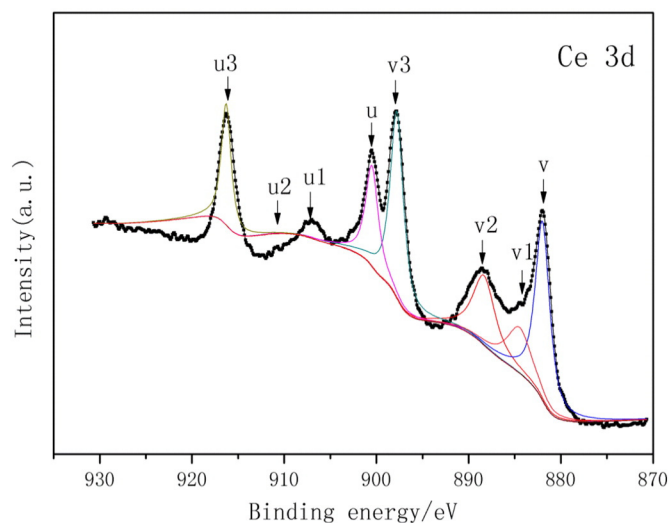


Fig. 5. XPS results of Ce 3d over La_{0.6}Ce_{0.4}FeO₃ sample.

provided by the manufacturer. Ce⁴⁺ tends to absorb SO₂ and form Ce(SO₄)₂, which could inhibit the poisoning effect of SO₂ to the LaFeO₃ perovskite [20]. Combined with the catalytic activity results, the presence of Ce⁴⁺ on the catalyst surface could increase the catalytic activity of the perovskite structure La_xCe_{1-x}FeO₃.

4. Conclusion

LaFeO₃ perovskite oxides were prepared and found to exhibit appreciable catalytic performance in NO reduction. Their catalytic activity decline sharply when SO₂ gases were added into the CO + NO reaction system. The SO₂ resistance of the catalyst was significantly increased after Ce substituting into the A-site of the LaFeO₃ perovskite. Because of the special redox property of Ce, the La_{0.6}Ce_{0.4}FeO₃ catalyst could absorb SO₂ without affecting its catalytic activity. According to the XRD patterns of catalyst samples, combined with the CO-TPR and SO₂-TPD results, La_{0.6}Ce_{0.4}FeO₃ maintains the original perovskite structure, while still exhibiting comparatively good reductive activity and remarkable SO₂ resistance. Thus, the substitution of Ce is the key factor to the improvement of SO₂ resistance in LaFeO₃ perovskite catalysts.

Acknowledgments

This study was supported by the Project of Low Concentration Sulfur Dioxide Flue Gas Treatment under Grant No. 738010004. The authors are grateful for the support of the Central South University and the valuable technical help of Dr. He.

Appendix A. Supplementary data

Supplementary data to this article can be found online at <http://dx.doi.org/10.1016/j.catcom.2016.03.005>.

References

- [1] Mengmeng Li, Vencon G. Easterling, Michael P. Harold, Appl. Catal. B. 184 (2016) 364–380.
- [2] Dimitrios K. Pappas, Thirupathi Boningari, Punit Boolchand, Panagiotis G. Smirniotis, J. Catal. 334 (2016) 1–13.
- [3] Ping Xiao, Ryan C. Davis, Xiaoying Ouyang, Jinlin Li, Arne Thomas, Susannah L. Scott, Junjiang Zhu, Catal. Commun. 52 (2014) 69–72.
- [4] C.N. Costa, A.M. Efstathiou, J. Phys. Chem. C 111 (2007) 3010–3020.
- [5] D.I. Kondarides, T. Chafik, X.E. Verykios, J. Catal. 191 (2000) 147–164.
- [6] M.A. Peña, J.L.G. Fierro, Chem. Rev. 101 (2001) 1981–2017.
- [7] C.H. Kim, G.S. Qi, K. Dahlberg, W. Li, Science 327 (2010) 1624–1627.
- [8] Z.B. Wu, R.B. Jin, H.Q. Wang, Y. Liu, Catal. Commun. 10 (2009) 935–939.
- [9] R.Q. Long, R.T. Yang, J. Am. Chem. Soc. 121 (1999) 5595–5598.

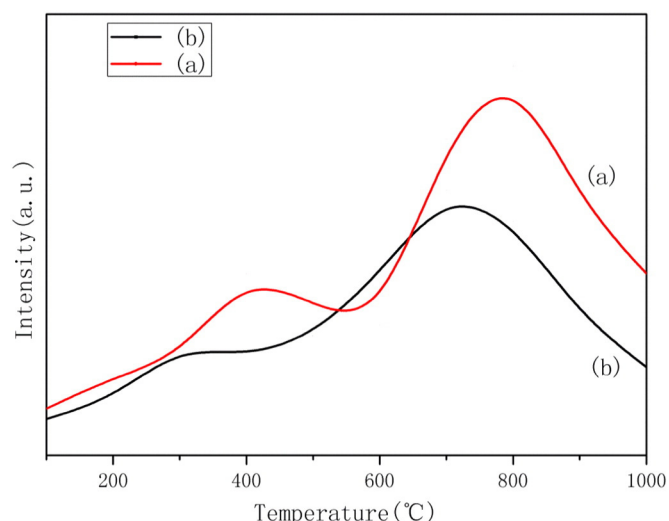


Fig. 4. SO₂-TPD profiles of the (a) LaFeO₃ and (b) La_{0.6}Ce_{0.4}FeO₃ samples.

- [10] B.M. Reddy, A. Khan, Y. Yamada, T. Kobayashi, S. Loidant, J.C. Volta, *J. Phys. Chem. B* 107 (2003) 5162–5167.
- [11] L. Chen, J. Li, M. Ge, *J. Phys. Chem. C* 113 (2009) 21177–21184.
- [12] S. Thirumalairajan, K. Girija, V. Ganesh, D. Mangalaraj, C. Viswanathan, N. Ponpandian, *Cryst. Growth Des.* 13 (2013) 291–302.
- [13] M. Daturi, G. Busca, *Chem. Mater.* 7 (1995) 2115–2126.
- [14] J.H. Chen, M.Q. Shen, X.Q. Wang, J. Wang, Y.G. Su, Z. Zhao, *Catal. Commun.* 37 (2009) 105–108.
- [15] J.J. Zhu, X.G. Yang, X.L. Xu, K.M. Wei, *Sci. China Ser. B* 50 (2007) 41–46.
- [16] B.P. Barbero, J.A. Gamboa, L.E. Cadús, *Appl. Catal. B* 65 (2006) 21–30.
- [17] C. Yanxin, J. Yi, L. Wenzhao, J. Rongchao, T. Shaozhen, H. Wenbin, *Catal. Today* 50 (1999) 39–47.
- [18] Dong Wook Kwon, Ki Bok Nam, Chang Hong Sung, *Appl. Catal. B* 166–167 (2015) 37–44.
- [19] W. Shan, F. Liu, H. He, X. Shi, C. Zhang, *Appl. Catal. B* 115–116 (2012) 100–106.
- [20] S. Yang, Y. Guo, H. Chang, L. Ma, Y. Peng, Z. Qu, N. Yan, C. Wang, J. Li, *Appl. Catal. B* 136–137 (2013) 19–28.